WELDING RESEARCH

SUPPLEMENT TO THE *WELDING JOURNAL*, DECEMBER 2000
Sponsored by the American Welding Society and the Welding Research Council

A New Ferritic-Martensitic Stainless Steel Constitution Diagram

New equivalency relationships improve the accuracy for predicting weld metal microstructure

BY M. C. BALMFORTH AND J. C. LIPPOLD

ABSTRACT. A new constitution diagram that more accurately predicts the microstructure of ferritic and martensitic stainless steel weld deposits has been developed. This diagram represents an improved version of the diagram presented by the authors in the January 1998 *Welding Journal* Research Supplement. Button melting and quantitative metallography techniques were used to produce additional microstructures, which supplied information about specific alloying element effects and provided microstructures near the phase boundaries, including the boundary for austenite formation. Using the entire database and linear regression analysis techniques, new equivalency formulae were developed and compared with existing formulae. Using the new equivalency formulae and iso-ferrite contour maps, a new ferritic-martensitic stainless steel constitution diagram was developed. Based on arc welds made using commercial martensitic and ferritic stainless steels, this diagram has proven to be extremely accurate in predicting weld metal microstructure within the composition limits of the diagram.

Introduction

The increasing popularity of ferritic and martensitic stainless steels in engineering applications over the past decade has focused considerable attention on the weldability of these alloys. The mechanical properties of the weld zone are very sensitive to microstructure, and poor microstructure control can limit their application. These microstructural effects, including the presence of ferrite in martensitic welds and martensite in ferritic welds, were summarized in a previous paper by the authors (Ref. 1).

Historically, constitution diagrams using chromium and nickel equivalents for the elements present in the alloy have served as road maps for determining weld deposit microstructure (or constitution). Most of the diagrams currently available, such as the WRC-1992 diagram, do not represent the constitution region for ferritic and martensitic stainless steels. Those that include the ferrite plus martensite region, such as the Schaeffler diagram, do not accurately predict microstructure. The objective of the work reported here was to develop a constitution diagram over a composition range that predicts weld deposit microstructures for ferritic and martensitic stainless steels with a higher degree of accuracy.

KEY WORDS

Constitution Diagram
Stainless Steel
Ferritic-Martensitic
Microstructure
Weld Metal
WRC-1992
Equivalency Formulas

As the compositional influence on weld microstructure is understood, greater confidence in utilizing ferritic and martensitic stainless steels will be possible. Development of a diagram that allows more accurate prediction of the compositional influence on weld microstructure will facilitate both alloy development and selection for welded applications and the choice of filler metals.

In an earlier paper (Ref. 1), a preliminary ferritic-martensitic stainless steel constitution was proposed. This diagram was based on an initial database produced by quantitative metallography and a large number of samples produced using a button melting technique. The preliminary diagram provided a rough estimate of weld metal microstructure, but further experimentation and evaluation were needed. The results reported here include a larger number of compositions that were produced by button melting in an effort to improve the accuracy of the preliminary diagram.

Experimental Approach and Procedures

The previous paper (Ref. 1) provides the details of the experimental procedures used to develop this diagram. The following sections are a summary of the procedures used.

Production of Alloy Buttons

Materials for this study included conventional, commercially available ferritic and martensitic stainless steels, along with other ferritic materials and grades of stainless steels. Some experimental compositions were also used. All of the chem-

M. C. BALMFORTH is with Dept. of Materials Science and Engineering, Massachusetts Institute of Technology, and was formerly with the Welding and Joining Metallurgy Group, The Ohio State University. J. C. LIPPOLD is with Welding and Joining Metallurgy Group, The Ohio State University, Columbus, Ohio.

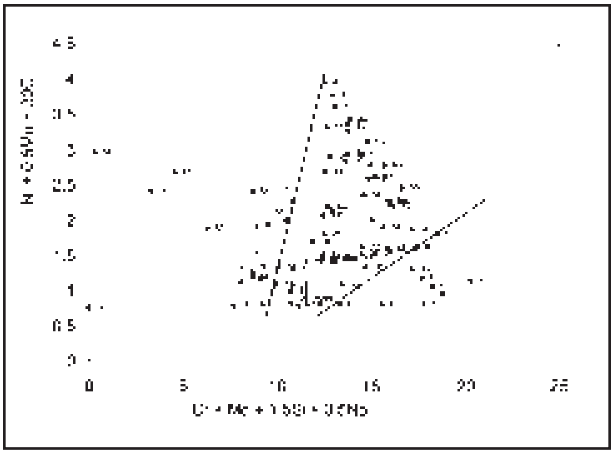

Fig. 1 — Button melt vol-% data plotted using the Schaeffler equivalents.

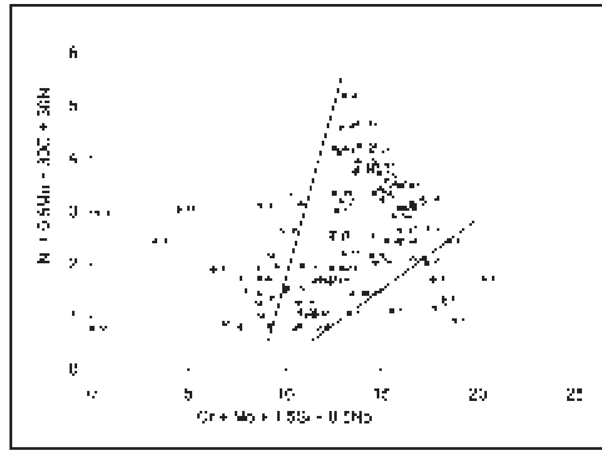

Fig. 2 — Button melt vol-% data plotted using the DeLong equivalents.

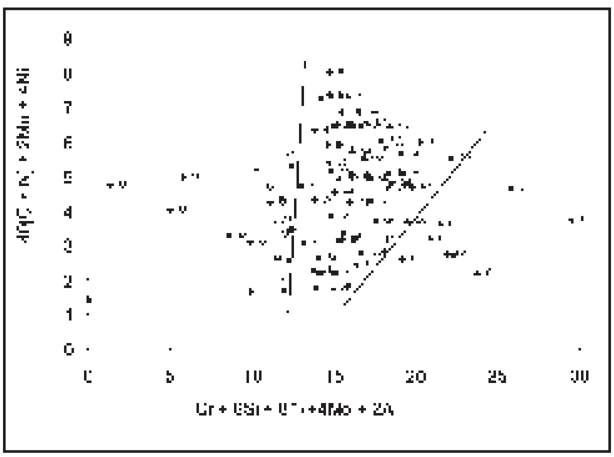

Fig. 3 — Button melt vol-% data plotted using the Kaltenhauser equivalents.

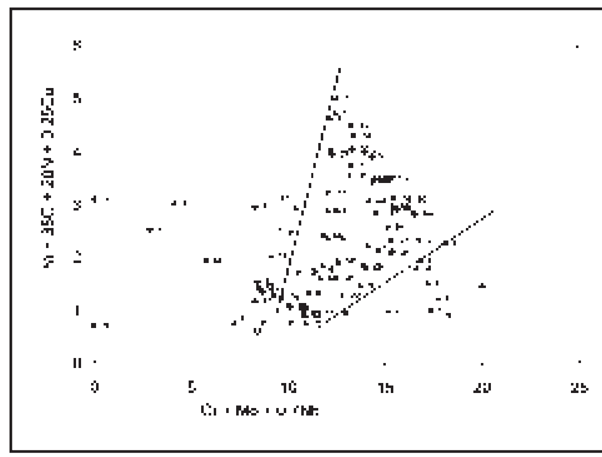

Fig. 4 — Button melt vol-% data plotted using the WRC-1992 equivalents.

ical compositions for the materials used were provided by the producers and are listed in Table 1. These base materials were combined in different dilutions in order to produce a range of microstructures. Other materials were used, in addition to the ferritic and martensitic stainless steels, in order to create combinations containing various amounts of alloying elements and microstructures bordering the duplex ferrite plus martensite constitution region.

Combinations of the base metals that would transect the duplex ferrite plus martensite constitution region were selected and mixed in different dilutions using a button melting technique. The button melts, which were used to simulate weld metal for microstructural data, were made by melting four grams of material, (*e.g.,* 3 g of one type of stainless steel with 1 g of another) in a water-cooled copper crucible using the GTAW process. It was confirmed in the earlier paper (Ref. 1) the button melting technique is a highly efficient and reliable method for simulation of weld metal and developing constitution diagrams.

The alloys were melted and allowed to cool under a high-purity argon-shielding atmosphere. Initially, dilutions of 25, 50 and 75% of each base metal were prepared. Button melts of the undiluted base metals were also made. Later, intermediate dilutions, such as 12.5%, were made in order to fill in appropriate areas on the diagram. The compositions of the individual buttons were estimated by dilution calculations based on the chemical compositions of the base materials. For example, if 1 g of Alloy A was combined with 3 g of Alloy B, the carbon content could be estimated by the following equation:

$$C_{button} = \frac{1(C_A) + 3(C_B)}{4}$$

where C_{button} = the carbon content of the button, C_A = the carbon content of alloy A and C_B = the carbon content of alloy B.

Characterization Techniques

Button melt specimens were sectioned in half using an abrasive wafering saw and ground and polished through colloidal silica. Three different etching techniques were employed to reveal the two-phase microstructures of these alloys. Most of the alloys responded well to an electrolytic etch using 10% oxalic acid in distilled water at 6 V for times up to 2 min. Some of the martensitic alloys were more easily characterized when immersed in Vilella's reagent (5 mL HCl, 1 g picric acid, 100 mL ethanol) for 3–4 s, and, in some of the two-phase alloys, martensite was much more visible, as a dark phase within light-colored ferrite, when swabbed for 1–2 s using Fry's reagent (5 g $CuCl_2$, 40 mL HCl, 30 mL water, 25 mL ethanol).

A colloidal suspension of Fe_3O_4 particles, known as ferro-fluid (Ref. 2), was used to determine whether austenite existed in specimens near the triplex austen-

Table 1 — Chemical Compositions of the Materials Used in This Study

	Composition, wt-%												
Alloy	C	Mn	Si	Cr	Ni	P	S	Al	Mo	Cu	Nb	Ti	N
Ferrite Stainless Steels													
409	0.018	0.28	0.49	11.54	0.14	0.023	0.001	—	—	—	—	0.18	—
444	0.02	0.36	0.23	17.85	0.37	0.031	0.001	—	1.92	—	0.33	0.33	0.019
430-A	0.046	0.45	0.38	16.48	0.27	0.026	0.003	0.005	0.09	0.08	—	0.003	0.046
430-B	0.036	0.47	0.31	16.1	0.11	—	—	—	0.02	0.08	—	—	0.035
430-C	0.04	0.44	0.42	16.6	0.21	0.024	0.001	0.003	0.17	0.08	0.017	—	0.035
439-A	0.02	0.3	0.4	17.89	0.2	—	—	—	0.04	0.07	0.48	0.41	—
439-B	0.012	0.27	0.28	17.32	0.32	0.031	0.001	0.064	0.039	0.074	0.01	0.33	0.012
409Ni	0.01	0.64	0.36	10.99	0.8	0.023	0.001	0.049	0.027	0.074	0.01	0.19	0.008
405	0.019	0.46	0.76	13.21	0.17	0.019	—	0.23	0.13	0.05	0.007	0.002	0.002
Martensitic Stainless Steels													
403-A	0.11	0.37	0.35	12.38	0.28	0.015	0.004	0.003	0.069	0.099	0.008	0.002	0.028
403-B	0.089	0.65	0.33	12.15	0.32	0.019	0.002	0.003	0.036	0.08	0.003	0.002	0.029
410	0.106	0.38	0.37	12.52	0.23	0.022	0.025	—	0.02	—	—	—	0.053
410Cb	0.122	0.24	0.29	12.0	0.17	0.023	0.007	—	0.03	0.09	0.174	0.002	0.008
410K	0.1	0.6	0.5	16.7	2.1	0.01	0.01	—	1.0	—	—	—	—
HT9	0.22	0.52	0.38	11.3	0.5	0.019	0.006	—	0.85	—	—	—	0.27
CC8	0.024	0.46	0.48	8.13	0.22	0.012	0.004	—	0.31	0.04	—	—	0.018
13Cr	0.031	0.389	0.155	12.88	3.96	0.012	0.002	—	1.01	—	—	—	0.02
Other Materials													
Fe	0.02	0.32	0.01	—	—	0.01	0.013	—	—	—	—	—	—
A36	0.088	0.627	0.236	—	—	0.005	0.025	—	—	—	—	—	—
304L	0.023	1.79	0.58	18.12	8.09	0.023	0.006	—	—	—	—	—	0.069
312	0.05	1.75	0.51	30.4	8.36	0.021	0.002	—	0.01	0.04	—	—	—
2205	0.014	1.46	0.48	22.16	5.64	0.028	0.001	—	3.04	—	—	—	0.18
21-6-9	0.067	8.31	0.29	20.16	7.03	0.017	0.003	0.018	0.22	0.072	0.001	0.002	0.197

ite-ferrite-martensite constitution region. Because the particles are ferromagnetic, they adhere to ferrite and martensite, giving a blue or brown color, while leaving austenite unaffected and white when observed with an optical microscope.

To determine the volume fraction of ferrite or martensite in the microstructures of the specimens, quantitative analysis was performed using the point-counting method according to ASTM E562.

Data Analysis

To determine which elements and their coefficients should be used in the new equivalency relationships for the prediction of volume-percent ferrite in ferritic and martensitic stainless steel welds, two linear regression techniques were used. Multiple linear regression, which analyzes relationships between one dependent variable and one or more independent variables, was used to determine the initial equations. Volume-percent ferrite was defined as the dependent variable, while the elements affecting ferrite content, such as nickel, chromium, nitrogen, etc., were defined as the independent variables. This process produces linear equations of the form:

$$\text{vol-\% ferrite} = C_0 + C_1(E_1)+C_2(E_2)+...+C_i(E_i) \quad (1)$$

where C_0 is a constant, the C_i terms are coefficients and the E_i terms are the elements included in the regression. Elements chosen for inclusion in the regression were based on previous equivalency formulae, experience and whether or not sufficient data existed for the element. Various combinations of elements were chosen, which produced a variety of equivalency relationships.

The various coefficients produced were evaluated using statistical methods, such as the standard deviation, T-value, P-value, R-squared value, and by examining the correlation matrix of the coefficients. Once the initial regressions were completed, ridge regression was used to improve the predictions for the coefficients. Ridge regression uses a ridge parameter (theta) to modify the least squares regression procedure to help avoid problems caused by highly collinear independent variables. As theta increases, biases in the coefficients increase, but the coefficients may be more precise. The goal is to find a small value of theta beyond which the estimates change slowly.

Chromium and nickel equivalent formulae developed during the regression analysis were then used to plot the volume-percent ferrite data. By plotting the various relationships and determining best-fit lines for the data, an iso-ferrite contour map was produced. The lines were drawn without curvature and were allowed to be nonparallel and non-equispaced.

Results and Discussion

Development of the New Diagram

After the preliminary diagram was proposed, more button melt samples were made in an attempt to fill in gaps where more microstructural data was needed. The data from these microstructures was then added to the existing database. All of the data from this work, including dilutions and phase ratios, are listed in the primary author's thesis (Ref. 3). The expanded data set was plotted, using existing equivalency formulae, as shown in Figs. 1 through 4. Only the equivalency relationships from the Schaeffler (Ref. 4), DeLong (Ref. 5), Kaltenhauser (Ref. 6) and WRC-1992 (Ref. 7) diagrams were used in these plots; the microstructure boundary lines from the original diagrams were not used. The boundary lines separating the martensite and ferrite regions from the two-phase region in the Figs. 1–4 were determined optimally. It is apparent boundary lines for determining 100% ferrite or martensite formation are possible using any of these equivalency relationships.

If guaranteeing either a fully ferritic or fully martensitic microstructure is all that is required, any of the diagrams in Figs. 1 through 4 would be sufficient. However, the addition of iso-ferrite lines to the diagram requires further analysis because the data is not distributed in a smooth transition from 0 to 100% within the two-

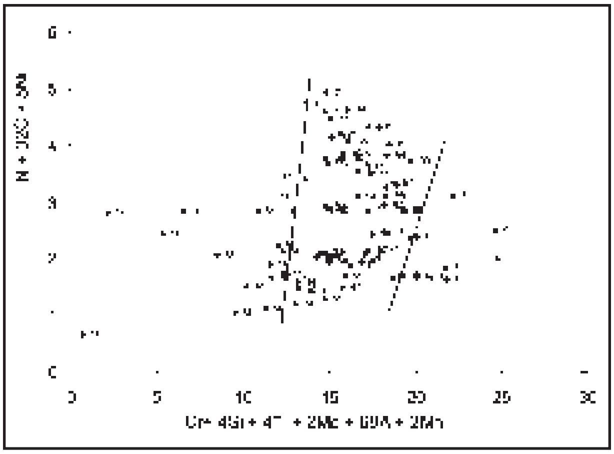

Fig. 5 — Button melt vol-% data plotted using experimental equivalents developed by linear regression analysis including the 0% and 100% data.

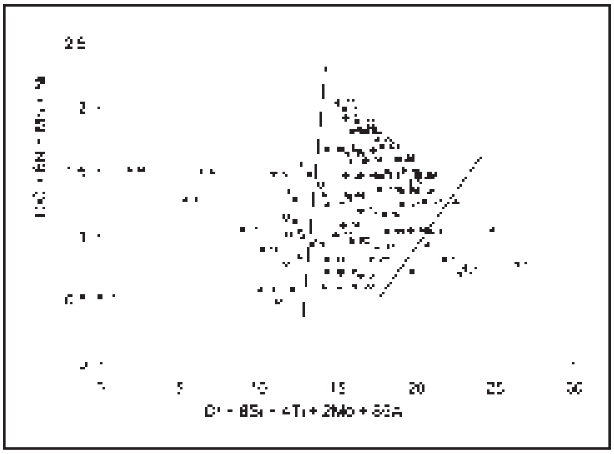

Fig. 6 — Button melt vol-% data plotted using experimental equivalents developed by linear regression analysis using only the two-phase data.

phase region.

Using linear regression analysis, few experimental equivalency relationships were determined, and the data was plotted, with these values for the axes, in Figs. 5 and 6. The equivalency relationships in Fig. 5 were determined using the complete data set, including the 0 and 100 vol-% ferrite data, while the equivalency relationships in Fig. 6 were determined using only the data from the two-phase microstructural region. It was felt that it was better to use only the two-phase data for the development of the constitution diagram. This is because the 0 and 100 vol-% data could be assigned to an entire region, not a specific point on the diagram, thus making this data less useful for the linear regression analysis. The equivalency relationships in Fig. 6 are similar to the Kaltenhauser factors, if the Kaltenhauser nickel relationship (40[C + N] + 2Mn + 4Ni) is divided by four, and with the exception of the overly large coefficient for aluminum.

At this point, the data analysis led to the conclusion that a diagram could be developed using new equivalency relationships developed with linear regression analysis. Also, by using the new equivalency relationships, iso-ferrite lines could be added within the two-phase region to provide a means of predicting weld metal constitution accurately within the ferrite plus martensite region.

Specific Alloying Element Effects

To resolve concerns over terms such as the coefficient for aluminum in Fig. 6, several buttons were made with specific alloying elements in mind. Alloys such as the nitrogen-strengthened austenitic stainless steel Nitronic 40 (21Cr-6Ni-9Mn-0.2N) and the duplex stainless steel 2205 were combined with the ferritic and martensitic stainless steels, as well as with pure iron and A36 structural steel, to create button melt samples with a range of nitrogen, manganese, aluminum and nickel contents. It was hypothesized that by producing a wider range of compositions, a more applicable coefficient could be determined for the element in question.

Austenite Formation

Another objective in the development of the diagram was to identify the boundary for austenite formation on the upper right side of the diagram. To do this, microstructures containing austenite were required. These were produced by mixing various alloys, such as austenitic Type 304L and duplex Type 312, mainly with ferritic stainless steels. Some austenite was also present in mixtures of 2205 with both ferritic and martensitic alloys. In collecting the microstructural data, a note was made if a microstructure was found to contain austenite, and this data was not used in the regression analysis. This data was later applied to the completed diagram in order to determine a boundary above which austenite can be expected to form in the weld metal.

These microstructures presented a challenge in determining whether austenite was present or whether the austenite had transformed to martensite on cooling. Some of the microstructures appeared very similar when etched using standard procedures. Alloys possessing a duplex ferritic/martensitic microstructure sometimes appear very similar to alloys with a duplex ferritic/austenitic microstructure. To determine whether austenite was present in these alloys, ferro-fluid color metallographic techniques were used (Ref. 2). Because austenite is not ferromagnetic, the iron particles in the ferro-fluid do not attach to it, and it appears white when observed under an optical microscope, while ferrite and martensite are colored blue or brown. The ferro-fluid technique was thus determined to be an efficient and reliable method for determining whether austenite was present in the microstructure.

Equivalency Relationships

With the addition of the new button melt data to the database, statistical predictions were improved significantly. Compositional ranges for the data were as follows: 7–20 Cr, 0.1–8 Ni, 0.01–0.6 Si, 0.01–0.22 C, 0.3–1.8 Mn, 0–0.23 Al, 0–0.33 Ti, 0–0.48 Nb, 0–3 Mo and 0–0.2 N. A total of 125 button melt samples were included in the database used for regression analysis. Multiple linear regression analysis was used to evaluate the alloying element effects on weld metal volume-percent ferrite. One of the predictive equations, developed using the same elements Kaltenhauser included in his ferrite factor, is given in the following:

$$\text{vol-\% ferrite} = -109 + 14.3(Cr + 2[Si + Mo] + 9[Al + Ti]) - 21.7(Ni + 20C + 10N + 0.3\,Mn) \quad (2)$$

The chromium and nickel equivalency relationships are the terms in parentheses. Various combinations of elements were chosen, based on previous equivalency formulae, experience and whether or not sufficient data existed for the element, producing a variety of equivalency relationships. From these regressions, coefficients were determined for several of the elements in the chromium and nickel equivalency formulae.

The coefficient of 2 for molybdenum was consistent throughout the regressions on various combinations of elements. Aluminum and titanium also had coefficients consistently in the 8 to 10 range. In most of the trials, carbon was stronger as an austenite stabilizer than nitrogen. The C:N ratio of around 1:5 found in the development of the WRC-1988 diagram (Ref. 8) seemed to apply here also. Coefficients of around 20 for carbon and 12 for nitrogen were common. Coefficients determined for chromium and nickel were statistically significant, with relatively small standard deviations. Chromium and carbon always showed the strongest effect on volume-percent ferrite.

Coefficients for manganese and silicon were not as consistent and left a degree of uncertainty. Each of these had small coefficients, and thus effects, on the volume-percent ferrite. Also, each was present in both the chromium and nickel equivalency relationships when included in various combinations with other elements. A very surprising finding was that niobium ended up with a negative coefficient, suggesting it acted as an austenite stabilizer, with values ranging from 2 to 8. A coefficient for copper was also investigated, but insufficient data and uncertain results precluded its inclusion in the equivalency relationships.

Because of these uncertainties and inconsistencies with other equivalency formulae, further evaluation was needed for some of the coefficients. Using the combinations of elements that made the most sense from the previous analysis, the correlation matrix of coefficients was examined. It was determined that some of the estimates of coefficients could have errors that were inflated from correlation with other element effect estimates. For example, niobium was strongly correlated to the titanium effect estimate. This means the coefficient for niobium was masked by the effect of titanium. This is a possible explanation why niobium seemed to have a negative coefficient. Nickel and molybdenum also showed possible inflation of the standard deviation error due to correlation with other effect estimates.

To evaluate these compositional effects further, ridge regression was employed. This technique, which improves the coefficient estimates by helping to avoid problems caused by highly collinear independent variables, was used to look for coefficients for niobium, silicon and manganese, and to determine if there was inflation of errors for nickel and molybdenum. This analysis showed a coefficient for niobium could not be determined with this data set. Coefficients for silicon and manganese were still uncertain. Also, the coefficients for nickel and possibly molybdenum could be reduced slightly. Reducing the nickel coefficient would have the effect of increasing the coefficients for carbon and nitrogen and other austenite stabilizers in the nickel equivalent relationships.

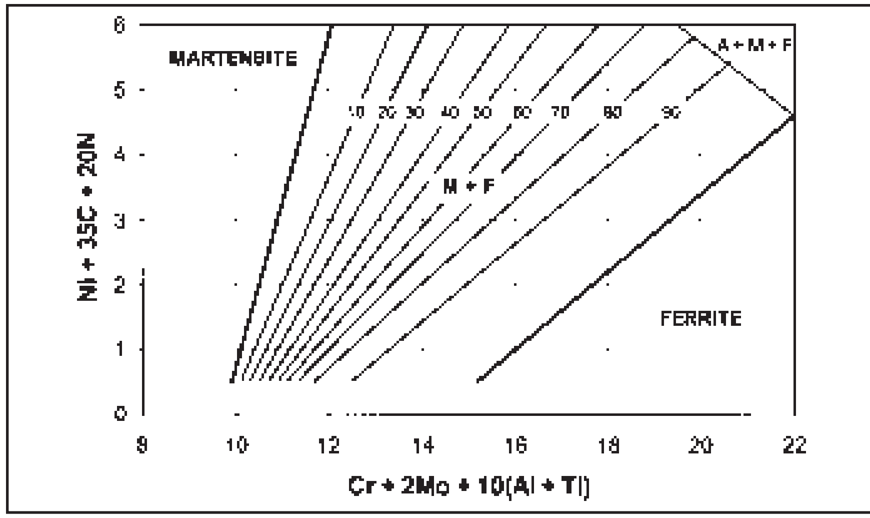

Fig. 7 — New ferritic-martensitic stainless steel constitution diagram, which contains a boundary for austenite formation. Iso-ferrite lines are in vol-% ferrite.

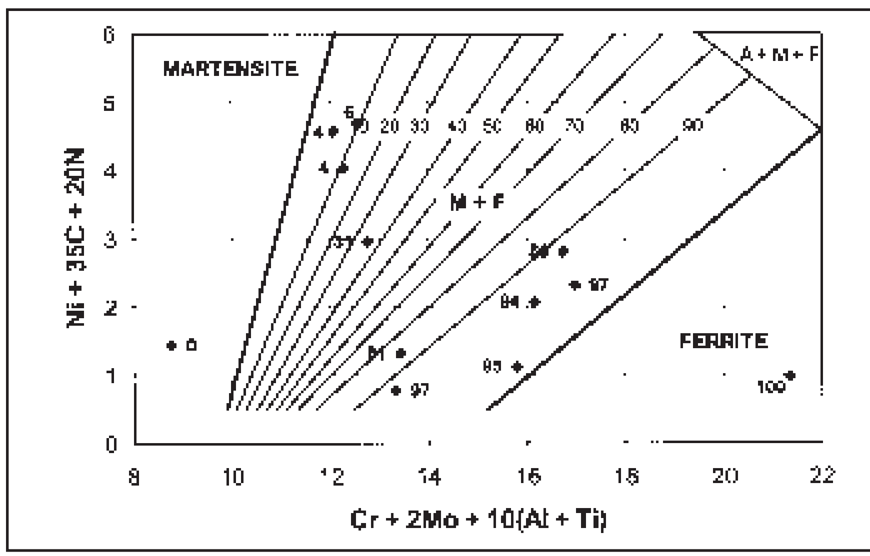

Fig. 8 — GTA weld vol-% ferrite data plotted on the new diagram.

Plotting the Data

Using the above information, several potential equivalency relationships were determined, and the chromium and nickel equivalent values were calculated for the button melt samples. The chromium and nickel equivalent values were then plotted with the volume-percent ferrite as the data label for each point. By plotting the various relationships and determining best-fit lines for the data, iso-ferrite contour maps were produced. If only the equations developed using linear regression analysis were used, they would produce a diagram with equispaced and parallel lines. The contour maps had lines that were not parallel or equispaced and that were based on actual data, thus potentially increasing the predictive accuracy. The iso-ferrite contour maps were then used to determine the best equivalency relationships.

On the basis of these evaluations, the best nickel and chromium equivalent equations were the following:

$$Cr_{eq} = Cr + 2Mo + 10[Al + Ti] \qquad (3)$$

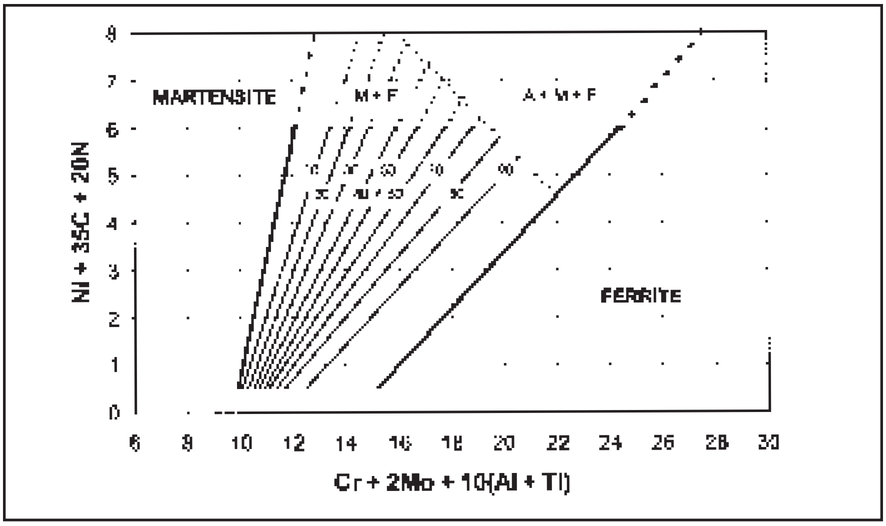

Fig. 9 — New ferritic-martensitic stainless steel constitution diagram with slightly extended axes.

and

$$Ni_{eq} = Ni + 35C + 20N \quad (4)$$

Although only the two-phase volume-percent ferrite data was used in the linear regression analysis, the data for 0 and 100 vol-% ferrite were included in plotting the diagram. This allowed boundary lines to be determined accurately, along with iso-ferrite lines within the two-phase region. All of the iso-ferrite lines were approximated as straight lines.

Austenite Boundary

Some of the button melt samples were mixed in dilutions that would form austenite in the microstructure. These data points were plotted using the new equivalency relationships, and a boundary where austenite begins to form was added to the diagram. Most of the data for austenite formation fell outside the region of volume-percent data and was thus not useful for inclusion in the new diagram. However, enough data existed to add a boundary to the upper right corner of the diagram.

New Diagram

The ferritic-martensitic stainless steel constitution diagram developed in this study is presented in Fig. 7. The iso-ferrite lines are in volume-percent ferrite. The equivalents were developed based on linear regression analysis and previous experience and intuition. Notice the nickel equivalent is identical to the WRC-1988 nickel equivalent (Ref. 8). Because the ridge regression technique suggested lowering the coefficient for nickel, the larger coefficients for carbon and nitrogen were chosen, and it was felt it would be best to have the diagram as much in agreement with the WRC equivalents as possible.

The shape of the martensite plus ferrite region is similar to the Schaeffler diagram (Ref. 4). The martensite boundary has a steeper slope than the ferrite boundary line. This trend also carries over from the Lefevre diagram (Ref. 9) and Lippold's ferritic stainless steel constitution diagram (Ref. 10). The iso-ferrite lines gradually change from steeper to lower slope as volume-percent ferrite increases.

For higher alloyed stainless steels where austenite formation is a possibility, an austenite boundary line has been included.

Evaluation of the New Diagram

__Verification with Actual Welds__

To check the accuracy of the new ferritic-martensitic stainless steel constitution diagram, autogenous GTA welds were made in all of the base metals used in this study, and volume-percent ferrite was determined for each. An autogenous square-groove weld was also made between Types 410Cb and 409Ni, giving a 50% dilution weld. This procedure helped verify the point counting technique for determining volume-percent ferrite in these alloys, as several of the button melt samples and actual welds were found to contain the same fraction of ferrite in the microstructure by point counting. In the plate materials, heat inputs of 20 and 40 kJ/in. were used. This, combined with the low heat inputs used for the sheet materials, ensured that the range of conventional arc welding heat inputs was represented. It was found that, within this range, the heat input did not greatly affect the volume-percent ferrite, and hence the predictive capability of the new diagram.

The weld data was then plotted on the new diagram, as shown in Fig. 8. It can be seen the weld metal volume-percent ferrite is predicted with a reasonable degree of accuracy by the new diagram. Further verification should be conducted using welds in alloys not used for production of button melt samples, but all of the available alloys were used in this study. It is felt, however, the microstructures of most conventional ferritic and martensitic stainless steel welds can be predicted accurately with the new diagram.

__Practical Implications__

The new ferritic-martensitic stainless steel constitution diagram provides a significant improvement over existing methods for predicting weld metal volume percent ferrite in these alloys. The database used in its development was more extensive than that used by Lefevre (Ref. 9) or Lippold (Ref. 10), and the alloys were from the microstructure region of interest, unlike the Schaeffler diagram (Ref. 4), which was developed using austenitic alloys.

Because most constitution diagrams have been developed based on measured chemical compositions, there was a question whether using composition values based on dilution calculations would be accurate. As a check, the actual chemical compositions of several of the button melt samples were measured. A simple investigation, using the measured nitrogen values in place of the nitrogen values estimated by dilution calculations for the nickel equivalent values, was performed. It was determined the slight differences between measured values and estimated values were negligible in determining the volume-percent ferrite predicted by the diagram. When using the new diagram, the final microstructure of a dissimilar weld or weld with filler metal can be predicted by estimating the dilution and using the chemical composition of the base materials to calculate the final weld metal composition with dilution calculations.

Table 2 provides a comparison of weld metal constitution (volume-percent ferrite) between the Schaeffler diagram and the new diagram, and that determined metallographically for autogenous welds in Type 409 and Type 410 and a dissimilar combination between A36 and Type 430. It is evident the new diagram predicts weld metal microstructure much more accurately than the Schaeffler diagram in the ferrite plus martensite region.

Table 2 — Predicted vs. Actual Volume Percent Ferrite

Alloy	Phrase Field (Schaeffler)	Vol-% Ferrite (Schaeffler)	Vol-% Ferrite (Actual)	Vol-% Ferrite (New Diagram)
410	M + F	30	8	8
409	M + F	90	99	96
635 430 + 37% A36	M + F	20	0	0

It is felt the boundary lines for 100% ferrite and martensite on the new diagram are highly accurate, while the iso-ferrite lines are more qualitatively accurate. Also, the austenite formation boundary is considered qualitative. The diagram can be used with a high level of confidence to determine whether or not a second phase will form when welding the ferritic and martensitic stainless steels, and provides an accurate estimate of the actual volume-percent of the second phase. Figure 9 shows the new diagram with slightly extended axes. This was done to allow the diagram to be used when welding alloys, such as the 25Cr ferritics, whose base metal compositions fall outside the initial boundaries. Prediction of weld metal volume-percent ferrite or martensite above Ni_{eq} = 6 should be considered qualitative.

__Limitations__

The new diagram should only be applied to alloys welded with conventional arc welding processes. High-energy-density (HED) processes, such as laser beam welding (LBW) or electron beam welding (EBW), produce high solidification and cooling rates. Under these conditions, both the solidification and phase transformation behavior may be altered relative to arc welds. This may result in different proportions of ferrite and martensite and could promote the retention of austenite in some alloys.

Extrapolation of the lines on the diagram outside the boundary regions shown in Fig. 9 is not recommended. The microstructure database used in the development of the diagram is represented by the axes of the diagram; therefore, errors may be introduced by predicting microstructures outside the boundaries of the diagram. Prediction below Ni_{eq} = 0.5 is also not recommended. Microstructures of alloys containing very low carbon contents may not be accurately predicted by the new diagram. The diagram is very accurate within the compositional limits of conventional ferritic and martensitic stainless steels. A compositional range of confidence is listed in Table 3. The differences between the compositional values listed in Table 3 and those previously listed in the Equivalency Relationships section are due to the wide range of experimental data. The previously listed ranges were from the specific compositions of the experimental button melts, which included other types of stainless alloys and some non-stainless alloys. The compositional ranges listed in Table 3 are based more on commercially available ferritic and martensitic stainless steels.

Conclusions

1) A new ferritic-martensitic stainless steel constitution diagram is proposed that uses compositional factors developed using linear regression analysis. This new diagram includes iso-ferrite lines within the martensite plus ferrite region. A boundary for austenite formation is also proposed.

2) The diagram provides improved predictive accuracy over currently available methods for predicting ferritic and martensitic stainless steel weld metal microstructure. The boundary lines for 100% ferrite and martensite on the new diagram are highly accurate, while the iso-ferrite lines and austenite formation boundary are qualitatively predictive.

3) The new diagram should be applied only to alloys welded with conventional arc welding processes. The use of high-energy-density processes, such as laser and electron beam welding, may result in different proportions of ferrite and martensite and could promote the retention of austenite.

Acknowledgments

The authors acknowledge the American Welding Society, which provided principal funding for this project through an AWS graduate research fellowship. We are grateful to Damian Kotecki of The Lincoln Electric Co., who provided assistance and expert advice during the project. Thanks also to Paul Lovejoy, formerly with Allegheny Ludlum, for providing materials and advice, and others who provided materials, including Mauro Losz at Armco Research, Terry DeBold at Carpenter Technologies, Bryan O'Neal at Air Liquide and Ravi Menon at Stoody Company. We are appreciative of the Edison Welding Institute for allowing the use of the button melting equipment. We are also indebted to Professor Theodore T. Allen at The Ohio State University for his help with statistical analysis and interpretation.

Table 3 — Compositional Range of Confidence for the New Diagram

Element	Compositional Range (wt-%)
Cr	11–30
Ni	0.1–3.0
Si	0.3–1.0
C	0.07–0.2
Mn	0.3–1.8
Mo	0–2.0
Al	0–0.3
Ti	0–0.5
N	0–0.25

References

1. Balmforth, M. C., and Lippold, J. C. 1998. A preliminary ferritic-martensitic stainless steel constitution diagram. *Welding Journal* 77(1): 1-s to 7-s.

2. 1989. *ASM Handbook*, Volume 9, Metallography and Microstructures, John Newby, Ed. ASM International, Materials Park, Ohio.

3. Balmforth, M. C. 1998. Development of a ferritic-martensitic stainless steel constitution diagram. Master's thesis. Columbus, Ohio, The Ohio State University.

4. Schaeffler, A. L. 1949. Constitution diagram for stainless steel weld metal. *Metal Progress* 56(11): 680–680B.

5. DeLong, W. T., Ostrom, G. A., and Szumachowski, E. R. 1956. Measurement and calculation of ferrite in stainless steel weld metal. *Welding Journal* 35(11): 521-s to 528-s.

6. Kaltenhauser, R. H. 1971. Improving the engineering properties of ferritic stainless steels. *Metals Engineering Quarterly* 11(2): 41–47.

7. Kotecki, D. J., and Siewert, T. A. 1992. WRC-1992 constitution diagram for stainless steel weld metals: a modification of the WRC-1988 diagram. *Welding Journal* 71(5): 171-s to 178-s.

8. Siewert, T. A., McCowan, C. N., and Olson, D. L. 1988. Ferrite number prediction to 100 FN in stainless steel weld metal. *Welding Journal* 67(12): 289-s to 298-s.

9. Lefevre, J., Tricot, R., and Castro, R. 1973. Noveaux aciers inoxyables a 12% de chrome. *Revue de Metallurgie* 70(4): 259.

10. Lippold, J. C. 1991. A review of the welding metallurgy and weldability of ferritic stainless steels. EWI Research Brief B9101, Columbus, Ohio.